Scaling hyporheic exchange and its influence on biogeochemical reactions in aquatic ecosystems

Ben L. O'Connor[1] and Judson W. Harvey[1]

Received 14 May 2008; revised 8 September 2008; accepted 25 September 2008; published 17 December 2008.

[1] Hyporheic exchange and biogeochemical reactions are difficult to quantify because of the range in fluid-flow and sediment conditions inherent to streams, wetlands, and nearshore marine ecosystems. Field measurements of biogeochemical reactions in aquatic systems are impeded by the difficulty of measuring hyporheic flow simultaneously with chemical gradients in sediments. Simplified models of hyporheic exchange have been developed using Darcy's law generated by flow and bed topography at the sediment-water interface. However, many modes of transport are potentially involved (molecular diffusion, bioturbation, advection, shear, bed mobility, and turbulence) with even simple models being difficult to apply in complex natural systems characterized by variable sediment sizes and irregular bed geometries. In this study, we synthesize information from published hyporheic exchange investigations to develop a scaling relationship for estimating mass transfer in near-surface sediments across a range in fluid-flow and sediment conditions. Net hyporheic exchange was quantified using an effective diffusion coefficient (D_e) that integrates all of the various transport processes that occur simultaneously in sediments, and dimensional analysis was used to scale D_e to shear stress velocity, roughness height, and permeability that describe fluid-flow and sediment characteristics. We demonstrated the value of the derived scaling relationship by using it to quantify dissolved oxygen (DO) uptake rates on the basis of DO profiles in sediments and compared them to independent flux measurements. The results support a broad application of the D_e scaling relationship for quantifying coupled hyporheic exchange and biogeochemical reaction rates in streams and other aquatic ecosystems characterized by complex fluid-flow and sediment conditions.

Citation: O'Connor, B. L., and J. W. Harvey (2008), Scaling hyporheic exchange and its influence on biogeochemical reactions in aquatic ecosystems, *Water Resour. Res.*, *44*, W12423, doi:10.1029/2008WR007160.

1. Introduction

[2] Near-surface sediments in aquatic ecosystems are critical in terms of many biogeochemical reactions such as nitrification and denitrification, as well as gross primary productivity and community respiration [e.g., *Mulholland et al.*, 2001; *Peterson et al.*, 2001]. The sediment-water interface is an assemblage of mineral particles, organic and biogenic material, biological communities, and void spaces producing a complex three-dimensional environment that serves as a boundary for fluxes of water, solutes, and particulate matter to occur. Fluid-flow and sediment conditions control the transfer of reactive solutes, particles, and biota across the sediment-water interface to depths of several centimeters, and the gradients of these environmental factors control biogeochemical processes in sediments [*Huettel et al.*, 2003]. Aquatic ecosystems contain a wide range of fluid-flow and sediment characteristics that generate complex transport conditions composed of diffusive, advective, shear, and turbulent processes. These simultaneous transport mechanisms produce log-scale variability in hyporheic residence times and spatial variability in the environmental factors that control biogeochemical processes, which is why hyporheic exchange is considered to exert primary control over the net ecosystem response of biogeochemical processes in sediments [*Findlay*, 1995].

[3] Measuring biogeochemical reaction rates is difficult because of the small-scale over which many microbial-mediated reactions occur. Small-volume pore water samplers produce solute concentration gradients on the scale of centimeters in stream beds [*Harvey and Fuller*, 1998]. For finer spatial-scale resolution, microsensor technology provides direct measurements of environmental variables in near-surface sediments [e.g., *Revsbech et al.*, 2005]. Concentration profiles across the sediment-water interface are used to infer biogeochemical reaction rates using models with various terms that simulate transport within sediments, which include molecular diffusion, bioturbation, advection, dispersion, and groundwater mixing [*Bouldin*, 1968; *Boudreau*, 1984; *Berg et al.*, 1998; *Harvey and Fuller*, 1998]. These models are typically empirical and are not easily transferable to other aquatic systems, or even the same system undergoing changes in fluid-flow and sediment conditions.

[4] Interpreting reaction rates from concentration profiles requires quantifying the transport mechanism within sedi-

[1]U.S. Geological Survey, Reston, Virginia, USA.

ments. There has been substantial work in this area for coastal flat and marine ecosystems where the sediments are often muddy or sandy, and fairly uniform in particle sizes. For fine particle-sized sediments found in these systems, as well as many lake sediments, the dominant transport mechanism is molecular diffusion. The molecular diffusion coefficient in the sediments (D'_m) has been quantified using the molecular diffusion coefficient (D_m) modified to accommodate the tortuosity between sediment grains, as well as factors such as bioturbation and dispersion [*Boudreau*, 1984]. The parameterization of the D'_m in this manner introduces empirical variables that can be difficult to quantify, but its use in interpreting concentration profiles has provided insights on the depth distribution of biogeochemical reactions in sediments [e.g., *Revsbech et al.*, 1981; *Nielsen et al.*, 1990; *Thamdrup et al.*, 1994].

[5] Research in the area of hyporheic exchange processes provides an alternative description of transport in sediments with higher permeabilities. *Savant et al.* [1987], *Thibodeaux and Boyle* [1987], *Harvey and Bencala* [1993], and *Huettel et al.* [1996] demonstrated advective transport through sediments using solute tracers and hydraulic measurements that showed distinct flow patterns entering sediments and returning to the water column a short distance away. This advective transport mechanism is referred to as "pumping" where fluid-flow above the sediments generates a pressure distribution at the sediment-water interface driving flow into and out of the permeable sediments. The most frequently used model based on advective pumping [*Elliott and Brooks*, 1997a] assumes a sinusoidal pressure distribution at the sediment-water interface, and has been used to analyze the results of flume investigations examining hyporheic exchange for conditions of fairly uniform sand sediments and regularly shaped bed forms [e.g., *Elliott and Brooks*, 1997b]. More recent studies have examined the pumping mechanism experimentally under conditions of varying bed form geometries [*Marion et al.*, 2002], variable hydraulic conductivity [*Salehin et al.*, 2004], and within gravel sediments [*Tonina and Buffington*, 2007] where turbulence is likely to govern transport in the near-surface sediments.

[6] While the pumping model focuses on transport occurring below the sediment-water interface, research on transport in porous media has examined the momentum balance of the overlying flow and inside the sediments. This analysis requires a model that can produce continuity in velocity, shear, and pressure across the sediment-water interface. Connecting the momentum equation in the overlying flow with that in the porous sediment bed has been done by incorporating a conceptual boundary layer, referred to as the Brinkman layer in the near-surface sediments, which produces additional flow resistance terms and continuity in flow variables at the sediment-water interface [*Dade et al.*, 2001]. This model of hyporheic exchange is referred to as the "slip flow" model. The boundary condition that connects the overlying flow and the porous sediment bed introduces variables relating to the velocity distribution within the Brinkman layer that need to be related to the overlying flow and sediment characteristics empirically. *Beavers and Joseph* [1967] quantified the slip velocity (u_s) at the sediment-water interface as being proportional to the velocity gradient in the overlying flow with pore-averaged velocities decaying rapidly within the Brinkman layer to the Darcy velocity. The decay of velocity within the Brinkman layer is mediated through additional resistance terms introducing an effective viscosity (ν_e) within the sediment, which was found not to vary substantially with depth in the sediments [*Ruff and Gelhar*, 1972]. More recently, ν_e was interpreted as an effective diffusion coefficient (D_e), which was formulated using the slip flow model of *Ruff and Gelhar* [1972] using velocity profile measurements to quantify u_s [*Fries*, 2007].

[7] Natural aquatic systems tend to have spatially and temporally variable fluid-flow and geomorphic conditions that generate heterogeneity in the factors controlling hyporheic exchange. Parameterizing the variables in the pumping and slip flow models has only been applied to simplified fluid-flow, sediment, and bed geometry conditions, which makes application to natural systems difficult. A recent numerical modeling investigation of hyporheic exchange used computational fluid dynamic simulations to quantify the pressure distribution over irregularly shaped bed forms coupled to flow governed by Darcy's law in the sediments [*Cardenas and Wilson*, 2007]. This type of analysis has improved upon the *Elliott and Brooks* [1997a] pumping model that assumed simplified conditions at the sediment-water interface (i.e., sinusoidal pressure distribution and a flat bed). While this numerical modeling approach is revealing about the controlling processes of hyporheic exchange, it is not an easily applied tool that can be used to interpret empirical biogeochemical profiles. Another issue with this model is that it defines a sharp boundary between the fluid-flow in the water column and advective Darcy flow in the sediments, which does not account for the penetration of turbulent eddies into the sediment pore space for beds with larger particle sizes [*Nagaoka and Ohgaki*, 1990].

[8] The reality for complex natural systems is that a combination of processes including molecular diffusion, advective pumping, shear-driven flow, and turbulence penetration control surface and hyporheic water mixing. The net hyporheic exchange via these fundamental processes can be represented most simply as an effective diffusion mechanism, where D_e is quantified by the measurement of a conservative tracer between the water and sediments. *Richardson and Parr* [1988] and *Packman and Salehin* [2003] have related tracer-derived D_e values to variables describing fluid-flow and sediment characteristics in attempt to develop predictive scaling equations for hyporheic exchange. However, the data sets used in these investigations were limited to fairly narrow ranges in fluid-flow and sediment conditions. There is also some uncertainty between these studies with regards to which flow and sediment variables best characterize transport. For example, it is not clear whether fluid-flow conditions should be quantified using the average velocity (U) or the shear stress velocity (u_*), or whether sediments should be characterized by permeability (K), hydraulic conductivity (K_c), or some variable describing the particle size distribution.

[9] The motivation for this study was to quantify hyporheic exchange in complex natural systems where a combination of transport mechanisms control fluxes, and to evaluate conditions for which simple advection-based models are applicable. Additionally, we wanted to develop a model for hyporheic exchange that could be used to

interpret reaction rates from biogeochemical profiles in natural systems (i.e., streams where hyporheic exchange is highly variable, and in advective nearshore marine systems) where the traditionally used molecular diffusion-based models are not always valid. In this investigation, we synthesized previous laboratory conservative tracer experiments and used dimensional analysis to scale D_e over a wide range of fluid-flow and sediment characteristics. The scaling relationship for D_e was used to interpret dissolved oxygen (DO) profiles in sediments from previous flume, open channel, and field investigations. The modeled DO reaction rates were compared to measured flux values to evaluate the reliability of D_e model. The use of a scaling relationship to quantify hyporheic exchange sacrifices a mechanistic understanding of the individual transport processes involved, in order to gain a more simple and robust transport model that can be applied over a wide range in fluid-flow and sediment conditions. The main benefit for this more simplified approach is in its application for examining empirical data addressing coupled biogeochemical-hyporheic exchange processes in near-surface sediments.

2. Background Information

[10] In this section we describe the basics of three commonly used hyporheic exchange models: effective diffusion, pumping, and slip flow. The effective diffusion model lumps together physical transport mechanisms into a single D_e coefficient, while the pumping and slip flow models primarily focus on advective transport within the sediments. There are alternative methods for quantifying hyporheic exchange such as a nonlocal exchange models [e.g., *Marinelli et al.*, 1998] and examination of sediment tracer breakthrough curves [e.g., *Reimers et al.*, 2004], which were not examined in this study.

2.1. Effective Diffusion

[11] Biogeochemical and transport processes across the sediment-water interface are three-dimensional in nature. However, for point measurements of biogeochemical gradients, the interpretation of process rates are often viewed from a one-dimensional perspective and multiple profiles with information on sediment topography can be used to capture spatial variability [e.g., *Røy et al.*, 2002]. Viewing transport as diffusion provides a direct means to evaluate biogeochemical gradients using a mass conservation formulation

$$\frac{\partial C}{\partial t} = \frac{\partial}{\partial y}\left(D_e \frac{\partial C}{\partial y}\right) - R \tag{1}$$

where C is concentration, t is time, and R is the net uptake rate (sum of production and uptake reactions). This type of model has been used to quantify biogeochemical processes such as photosynthesis and respiration rates by comparing DO profiles in sediments over time between light and dark cycles [e.g., *Revsbech et al.*, 1986]. For many biogeochemical processes of interest, a steady state form of equation (1) is suitable for interpretation of reaction rates and a numerical fitting algorithm PROFILE has been developed to evaluate microsensor profiles [*Berg et al.*, 1998].

[12] Molecular diffusion has often been assumed to be the driving transport mechanism when examining biogeochemical gradients in sediments [*Reimers et al.*, 2001]. The molecular diffusion coefficient (D_m) must take into account the diffusion around sediment particles, which has been examined theoretically [*Berner*, 1980], as well as empirically by relating the sediment tortuosity to measured electrical resistivity and sediment porosity (θ) [*Archie*, 1942]. Several studies have used these methods to derive expressions between tortuosity and θ [e.g., *Boudreau*, 1996], which can be used to generalize the expression for the molecular diffusion in sediments as

$$D_e = \beta D_m = D'_m \tag{2}$$

where β represents the empirical expression for tortuosity as a function of θ, and in this study we used

$$\beta = \frac{1}{1 + 3(1 + \theta)} \tag{3}$$

as described by *Iversen and Jørgensen* [1993]. In addition to molecular diffusion, the effects of bioturbation, turbulent diffusion, and dispersion have been included into the expression of effective diffusion

$$D_e = \beta(D_m + D_b) + D_d \tag{4}$$

where the biodiffusivity (D_b) and dispersion coefficient (D_d) must be obtained empirically or modeled [*Berg et al.*, 1998; *Güss*, 1998].

[13] A measured value for D_e over a sediment bed can be obtained directly by use of a conservative tracer. Consider a closed system (i.e., a recirculating flume) where the tracer concentration in the sediments (C) is initially zero, and the tracer concentration in the overlying water is $C_w = C_o$ (well-mixed system initially). Hyporheic exchange will drive a tracer into the sediment pore water resulting in a decrease of tracer concentration in the overlying water over time. Modeling hyporheic exchange as an effective diffusion process, the flux of tracer to the sediments is governed by Fick's second law

$$\frac{\partial C}{\partial t} = D_e \frac{\partial^2 C}{\partial y^2} \tag{5}$$

and with the well-mixed system approximation, the boundary conditions for equation (5) are: the concentration at the sediment-water interface is equal to C_o, and $\partial C/\partial y = 0$ deep in the sediments. A solution for equation (5) can be obtained for C assuming a semi-infinite domain and using Laplace transforms resulting in

$$C = C_o\left(1 - \mathrm{erf}\left(\frac{y}{2\sqrt{D_e t}}\right)\right) \tag{6}$$

as described by *Crank* [1975]. The flux of solute from the overlying water to the sediments is governed by Fick's first law

$$J = -D_e \left.\frac{dC}{dy}\right|_{y=0} \tag{7}$$

and taking the derivative of equation (6) at the sediment-water interface and inserting it into equation (7) gives an expression of the solute flux

$$J = C_o\sqrt{\frac{D_e}{\pi t}} \tag{8}$$

which is different from the work by *Packman and Salehin* [2003]; *Packman et al.* [2004] by a factor of $\sqrt{\pi}$ caused by an error in grouping terms in their derivation.

[14] The net solute flux can also be obtained by a mass conservation expression

$$J = -\frac{V_w}{A_s}\frac{dC_w}{dt} \tag{9}$$

where V_w is the volume of the overlying water in the recirculating system, A_s is the surface area of the sediment bed, and $C_w(t)$ is the solute concentration in the overlying water as a function of time. Equating equations (8) and (9), rearranging terms, and integrating results in

$$C_w = C_o\left(1 - 2\frac{A_s}{V_w}\sqrt{\frac{D_e t}{\pi}}\right) \tag{10}$$

which describes a linear decrease in solute concentration with respect to $t^{1/2}$. Experimental tracer data typically follows this linear behavior for initial time periods, but the decrease in C_w eventually decays over long time periods [*Marion et al.*, 2002]. The initial slope of a plot of C_w versus $t^{1/2}$ can be used to quantify D_e as

$$D_e = \left(\frac{\sqrt{\pi}}{2}\frac{V_w}{A_s}\frac{dC^*}{d(t^{1/2})}\right)^2 \tag{11}$$

where $C^* = C_w/C_o$ is the normalized solute concentration in the overlying water. The error in the expression for J (equation (8)) used by *Packman and Salehin* [2003] and *Packman et al.* [2004] propagates through in their formulation for D_e, which differs from equation (11) by a factor of π.

2.2. Pumping Model

[15] The pumping model presented by *Elliott and Brooks* [1997a] quantifies hyporheic exchange by examining the sediment domain of the problem. The continuity equation for steady flow in sediments, assuming isotropic sediments (constant hydraulic conductivity, K_c) follows Laplace's equation

$$\nabla^2 h = 0 \tag{12}$$

where h is the piezometric head ($h = p/\rho g$, where p is pressure and ρ is the density of water). The pressure field within the sediments is calculated assuming a sinusoidal head distribution at the sediment-water interface,

$$h(y=0) = h_m \sin\left(\frac{2\pi}{\lambda}x\right) \tag{13}$$

where λ is the bed form wavelength, x is the streamwise coordinate, and h_m is the half amplitude of the piezometric head variation at the sediment-water interface, which has been empirically derived as

$$h_m = 0.28\frac{U^2}{2g}\left(\frac{\Delta/H}{0.34}\right)^{\gamma} \tag{14}$$

where U is the average velocity, Δ is the bed form height, H is the water depth, and γ is an empirical constant ($\gamma = 3/8$ for $\Delta/H < 0.34$, and $\gamma = 3/2$ for $\Delta/H \geq 0.34$) [*Elliott*, 1990]. The resulting solution for the h distribution is

$$h = h_m \sin\left(\frac{2\pi}{\lambda}x\right)e^{-\frac{2\pi}{\lambda}y} \tag{15}$$

where y is the vertical coordinate. Darcy's law is used to calculate the seepage velocity field ($\mathbf{v}$, a volume average of the interstitial velocity) in the sediments and produces streamlines entering and exiting the sediments according to

$$\mathbf{v} = -\frac{Kg}{\nu}\nabla h \tag{16}$$

where K is the sediment permeability, g is the acceleration due to gravity, and ν is the kinematic viscosity.

[16] The net hyporheic exchange to the sediments is evaluated by assuming that the sediment bed is initially free of solute and the pumping model then tracks the accumulation of solute mass inside the bed over time. An average residence time function $\overline{R}(\xi)$ is introduced, which represents the fraction of solute that has remained in the sediment bed for an elapsed time ξ (for a more detailed description of $\overline{R}(\xi)$, see *Elliott and Brooks* [1997a, Appendix]). This accounts for the fact that solute is entering and exiting the sediments with a distribution of associated residence times. The flux of a solute into the sediment bed normalized by the solute concentration in the overlying water, C, is

$$q(x) = \begin{cases} \mathbf{v}\cdot\mathbf{n} & \text{if } \mathbf{v}\cdot\mathbf{n} \geq 0 \\ 0 & \text{if } \mathbf{v}\cdot\mathbf{n} < 0 \end{cases} \tag{17}$$

where $\mathbf{n}$ is the unit vector normal to the sediment-water interface. The average normalized flux, $\overline{q}$, is calculated by taking the average of the absolute value of $\mathbf{v}\cdot\mathbf{n}$ over the entire surface of the sediment bed. The accumulation of solute mass per unit area of the bed can be estimated as the convolution integral of the residence time function

$$M(t) = \overline{q}\int_{\xi=0}^{\infty}\overline{R}(\xi)C(t-\xi)d\xi \tag{18}$$

which tracks the mass accumulation inside the sediments. To get the net hyporheic exchange, information on $C(t)$ in the overlying water is measured and equation (18) is coupled to a mass conservation equation in the overlying water.

[17] The pumping model can be formulated to represent mass transfer by effective diffusion in the same manner used to derive equation (11) where the flux at the

interface according to Fick's second law was equated with the net solute flux derived from a mass balance on the recirculating water in the flume. The analogous expression to equation (10) describes the solute mass accumulation in the sediments

$$\frac{M'}{\theta} = 2\sqrt{\frac{D_e t}{\pi}} \tag{19}$$

where $M' = M/C_o$ and M'/θ is known as the effective depth of solute penetration. A plot of M'/θ versus $t^{1/2}$ has a linear increase initially and the slope can be used to quantify D_e as:

$$D_e = \left(\frac{\sqrt{\pi}}{2}\frac{d(M'/\theta)}{d(t^{1/2})}\right)^2 \tag{20}$$

[18] During the initial time period of a tracer experiment, *Elliott and Brooks* [1997a] showed that the convolution integral (equation (18)) can be approximated by

$$\frac{M'}{\theta} = \frac{3.5}{2\pi}\sqrt{\frac{K_c h_m t}{\theta}} \tag{21}$$

which is valid up to a point where the bed starts to become saturated with tracer. Combining equations (19) and (21) results in

$$D_e = \frac{1}{\pi\theta}\left(\frac{3.5}{4}\right)^2 K_c h_m \tag{22}$$

which represents an estimation of D_e using the pumping model with a sinusoidal pressure gradient at the sediment-water interface based only on sediment and fluid-flow variables.

2.3. Slip Flow Model

[19] The slip flow model depicts the transition in physics from the overlying fluid-flow to the porous media flow in the sediments. This means connecting the Navier-Stokes equation for the overlying flow and within the sediment pores at the microscale to Darcy's law in the porous sediment bed at the macroscale. Mathematically, this is a challenge as the Navier-Stokes equation is a second-order, nonlinear equation and in the overlying flow is expressed as

$$\frac{\partial \mathbf{u}}{\partial t} + \mathbf{u}\cdot\nabla\mathbf{u} = -\frac{\nabla p}{\rho} + \nu\nabla^2\mathbf{u} + \mathbf{F}_b \tag{23}$$

where $\mathbf{u}$ is the velocity vector field in the overlying flow, p is pressure, and $\mathbf{F_b}$ is the net body force (or gravity term in free surface problems). Darcy's law, which was empirically deduced but can also be derived from the Navier-Stokes equations through averaging over large pore volumes, is a first-order, linear equation

$$\frac{\nabla p}{\rho} = -\frac{\nu}{K}\mathbf{v} \tag{24}$$

which is the same as equation (16) written in terms of p instead of h. Some researchers have treated this problem using a single domain (overlying water and sediment bed) [e.g., *Basu and Khalili*, 1999]. *Zhou and Mendoza* [1993] started with equation (23) and used ensemble averaging to derive equations describing the macroscale transport within the sediment bed.

[20] A more basic approach to this two-domain problem involves only examining the sediment bed portion and including additional force terms to equation (24) in the fashion of *Beavers and Joseph* [1967] and *Ruff and Gelhar* [1972]. This requires the use of the conceptual Brinkman boundary layer just below the sediment-water interface. The characteristic length scale for the Brinkman layer is $\sqrt{K}$ [*Beavers and Joseph*, 1967] over which the additional flow resistance is generated by viscous shear stress and nonlinear form drag. The extended Darcy equation is formed with the addition of these terms as:

$$\frac{\nabla p}{\rho} = -\frac{\nu}{K}\mathbf{v} + \nu_e\nabla^2\mathbf{v} - \frac{C_D}{\sqrt{K}}\mathbf{v}^2 \tag{25}$$

The third term in equation (25) represents the Brinkman term and introduces an effective viscosity (ν_e). The fourth term in equation (25) represents the Forchheimer term where C_D is a dimensionless form drag coefficient, which is a property of the porous sediment bed [*Venkataraman and Rama Mohan Rao*, 1998]. *Ruff and Gelhar* [1972] solved for the $\mathbf{v}$ field using equation (25) with an empirically derived value for C_D and evaluating ν_e as both a constant and varying with depth. This solution for $\mathbf{v}$ also provided an expression of the slip velocity, u_s, tangential to the sediment-water interface (the slip velocity is on the water side of the interface and is not a volume average of the interstitial velocity). Their resulting expression for u_s assuming a constant ν_e was

$$\left(\frac{u_s}{u_*}\right)^3 + \frac{3}{2C_D Re_K}\left(\frac{u_s}{u_*}\right)^2 = \frac{3Re_K}{2C_D}\frac{\nu}{\nu_e} \tag{26}$$

where $Re_K = u_*\sqrt{K}/\nu$ is the Reynolds number characterizing flow within the Brinkman layer. *Fries* [2007] evaluated ν_e as an effective diffusion ($\nu_e \approx D_e$) in equation (26), which was rearranged as

$$D_e = \frac{3\nu Re_K^2}{2C_D Re_K u_{s+}^3 + 3u_{s+}^2} \tag{27}$$

where the dimensionless slip velocity, $u_{s+} = u_s/u_*$, was estimated by fitting measured velocity profiles to the Reichardt velocity profile.

2.4. Previous Studies Examining Effective Diffusion Model

[21] Hyporheic exchange is a result of a combination of processes, which is why several transport models have been developed to simulate and analyze empirical data. The three most commonly used transport models are the effective diffusion, pumping, and slip flow models presented previously. The pumping and slip flow model are mechanistic in that they quantify the physics of advective transport by making simplifications to the physical conditions of the problem. While the effective diffusion model uses the

Table 1. Summary of Sediment and Fluid-Flow Conditions for Hyporheic Exchange Data Sets

Study	d_g (mm)	K (10^{-6} cm^2)	θ	Δ (cm)	λ (cm)	u_* (cm s^{-1})	U (cm s^{-1})	H (cm)
Richardson[a]	0.1–3.0	0.17–71	0.36–0.40	0	0	0.3–1.3	3.7–22.9	0.6–1.9
Nagaoka[b]	19.0–40.8	500–2300	0.24	0	0	1.1–4.3	8.9–42.8	3.2–7.0
Lai[c]	0.5–3.2	2.3–19	0.36–0.38	0	0	0.2–0.6	7.4–15.4	0.5–2.0
Elliott[d]	0.1–0.5	0.08–1.1	0.30–0.33	1.1–2.5	9–30	1.3–2.4	8.6–13.2	3.1–6.5
Marion[e]	0.85	5.0	0.38	0–3.5	0–120	1.7–1.8	22.0–28.0	10.9–12.3
Packman[f]	4.8	150	0.38	0–3.7	0–32	1.1–3.2	9.0–36.1	11.3–20.5
Various[g]	0.5	0.68–1.8	0.29–0.38	0.8–1.9	15–70	0.5–1.7	12.0–23.7	7.1–12.7
Tonina[h]	9.8–10.8	51	0.34	3.6–12.0	515–560	3.8–5.5	28.2–46.0	3.9–10.4

[a] *Richardson and Parr* [1988], flat bed with glass sphere sediments.
[b] *Nagaoka and Ohgaki* [1990], flat bed with glass sphere sediments.
[c] *Lai et al.* [1994], flat bed with glass sphere sediments.
[d] *Elliott and Brooks* [1997b], bed forms with sand sediments.
[e] *Marion et al.* [2002], flat bed and bed forms with sand sediments.
[f] *Packman et al.* [2004], flat bed and bed forms with gravel sediments.
[g] *Packman et al.* [2000], *Packman and MacKay* [2003], *Ren and Packman* [2004], and *Rehg et al.* [2005], flat bed and bed forms with sand sediments.
[h] *Tonina and Buffington* [2007], bed forms with gravel sediments.

mathematics of diffusive transport, it is an empirical model as the transport parameter D_e represents the net transport by several processes and must be obtained from experimental data. Tracer tests provide a means to quantify D_e directly, but the only way to obtain D_e, a priori, is through the development of predictive correlations with respect to fluid-flow and sediment characteristics controlling hyporheic exchange.

[22] Scaling D_e to physical conditions governing transport requires thorough, multivariate analysis of the controlling variables. Previous scaling attempts have focused on relating D_e to a characteristic velocity and length scale relevant to the perceived transport mechanism controlling hyporheic exchange. *Richardson and Parr* [1988] performed tracer experiments in a flume with a flat bed of glass spheres. The mass transfer was assumed to be dominated by shear-induced flow (slip flow model) at the interface and they found that u_* and K best explained the variability in experimental D_e values according to $D_e = 6.59 \times 10^{-5} D_m (u_* \sqrt{K}/\nu)^2$. *Packman and Salehin* [2003] used dimensional analysis and available literature data to scale D_e to the Reynolds number ($Re = UH/\nu$) of the overlying flow, where U is the average velocity and H is the stream depth. This scaling resulted in power law relationship of $D_e \sim Re^2$ with varying intercepts for studies using different types of sediment particle sizes and bed form configurations. The velocity head term ($U^2/2g$) in equation (14) of the pumping model was interpreted as the cause of the observed Re^2 scaling. In a separate study involving a flat bed with gravel sized sediments, D_e was scaled to the particle Reynolds number ($Re_p = Ud_p/\nu$) [*Packman et al.*, 2004], which also demonstrated Re_p^2 scaling but with a better collapse in data from studies using different particle sizes and bed form configurations.

[23] These previous studies that examined the scaling of D_e have provided insight on some of the controlling variables affecting hyporheic exchange. However, these scaling relationships have not received much attention because they were developed using fairly limited data sets, and they lack validation in their application in predicting hyporheic exchange. More recently, *Marion and Zaramella* [2005] used a small set of published flume studies and demonstrated that the effective diffusion model accurately characterized hyporheic exchange for a broad, intermediate range of time periods relating to the exchange process. They also concluded that a depth-independent value of D_e is sufficient for the effective diffusion model in predicting hyporheic exchange.

3. Methods

3.1. Hyporheic Exchange Data Sets

[24] We compiled data from various flume tracer studies in order to examine the effects of varying fluid-flow and sediment conditions on transport in permeable sediments. The data sets are summarized in Table 1. The first task was to get a consistent set of measured D_e values from the tracer experiments, as well as fluid-flow and sediment conditions. The procedures used to calculate D_e vary somewhat between studies, depending upon how the tracer experiment was conducted. *Nagaoka and Ohgaki* [1990] used a salt tracer in the overlying water and conductivity probes at four depths and obtained D_e using equation (5). This type of measurement was possible because of the large, uniform particles used to make the bed (Table 1). *Richardson and Parr* [1988] and *Lai et al.* [1994] used a sediment bed saturated with a dye tracer of concentration $C_{o,s}$ and measured the mass accumulation of tracer in the overlying water column as a function of time. For this type of experiment, D_e was calculated using

$$D_e = \left(\frac{\sqrt{\pi}}{2C_{o,s}} \frac{dM_w}{d(t^{1/2})} \right)^2 \tag{28}$$

where M_w is the cumulative mass of dye transferred from the sediment to the water. The rest of the studies used a tracer, initially in the water column only, and tracked either the decrease of solute concentration in the water column (equation (10)), or the solute mass accumulation in the bed (equation (19)). For all studies, we used the plots of either mass or concentration versus the square root of time to compute the needed slopes in equations (11), (20), and (28) for calculating experimental D_e values.

[25] Reported variables relating to fluid-flow and sediment conditions included U, bed geometry, particle size distribution information, θ, and either K or hydraulic con-

ductivity (K_c). Shear stress velocity was either reported or obtained by using the normal flow estimation ($u_* = \sqrt{gHS}$, where S is the slope of the bed). Particle size distribution information was used to estimate the geometric mean particle size (d_g) and the particle size such that 90% of the particles are finer (d_{90}). The studies used a variety of sediment bed geometries that included flat beds, as well as those containing natural and regular bed forms characterized by the bed form wavelength (λ) and amplitude (Δ). Hyporheic exchange is affected by the bed geometry, so it is difficult to compare values between flat beds and those with bed forms. We used the definition of roughness height (k_s) described by *van Rijn* [1984]

$$k_s = 3d_{90} + 1.1\Delta\left(1 - e^{-25\Delta/\lambda}\right) \tag{29}$$

which provided a single variable for examining the effects of particle size and bed geometry on hyporheic exchange processes. Values of K or K_c were reported in most studies ($K = K_c\nu/g$) except for *Nagaoka and Ohgaki* [1990], which only gave information on particle size. For the Nagaoka study, K was estimated using the Kozeny-Carmen equation

$$K = 5.6 \times 10^{-3} \frac{\theta^3}{(1-\theta)^2} d_g^2 \tag{30}$$

which is one of the most widely used equations for predicting permeability for sediments with fairly uniform size distributions [*Freeze and Cherry*, 1979].

3.2. Dimensional Analysis

[26] Buckingham's Π theorem was used to generate dimensionless groupings of the controlling variables that involved three steps: (1) listing the minimum number of variables needed to describe hyporheic exchange, (2) generating dimensionless groupings of the controlling variables, and (3) using the compiled hyporheic exchange data set to determine a power law scaling relationship for D_e. The variables chosen for dimensional analysis represent the relevant fluid-flow and sediment conditions controlling hyporheic exchange according to both the pumping and slip flow models

$$D_e = f\left(D'_m, U, u_*, k_s, \sqrt{K}, \nu\right) \tag{31}$$

where D'_m is defined by equation (2) and includes θ; k_s is defined by equation (29) and includes the variables d_{90}, Δ, and λ describing the sediment bed. Equation (31) contains seven variables that are composed of two dimensions (L and T), which resulted in the possibility of $7 - 2 = 5$ dimensionless groupings. The five dimensionless groups were simplified to produce four groupings of dimensionless numbers known to affect hyporheic exchange

$$\frac{D_e}{D'_m} \sim \left(\frac{U}{u_*}\right), \left(\frac{u_* k_s}{\nu}\right), \left(\frac{u_*\sqrt{K}}{D'_m}\right) \tag{32}$$

where $U/u_* = C_z$ is the Chézy resistance coefficient, $u_*k_s/\nu = Re_*$ is the shear Reynolds number, and $u_*\sqrt{K}/D'_m = Pe_K$ is the permeability based Péclet number. Rewriting equation (32) with these dimensionless numbers in the form of a power law scaling results in

$$\frac{D_e}{D'_m} = \alpha C_z^a Re_*^b Pe_K^c \tag{33}$$

where α is a dimensionless constant. Individual correlations between D_e/D'_m and the dimensionless numbers (C_z, Re_*, and Pe_K) were used to determine the scaling exponents a, b, and c.

3.3. Dissolved Oxygen Data Sets

[27] We examined previous studies measuring DO profiles in sediments and compiled available information on fluid-flow and sediment conditions (see auxiliary material, Tables S1–S4).[1] Many of the DO profiles were measured in a stagnant or mixed chamber systems where estimating u_* was not possible. Also, it was uncommon to list detailed particle size distribution and in some cases, neither K or K_c was reported.

[28] Data from four investigations was used to assess the scaling relationship for quantifying D_e in interpreting uptake and production rates from DO concentration profiles. The experimental conditions for these four investigations include recirculating flumes [*Güss*, 1998; *O'Connor and Hondzo*, 2008b], a large-scale flow-through channel [*O'Connor and Hondzo*, 2008a], and field measurements taken within the south fork of the Iowa River located in central Iowa (B. L. O'Connor et al., unpublished data, 2007). The relevant sediment and fluid-flow conditions for these studies are listed in Table 2. The DO concentration profiles from the Iowa River were performed in a similar fashion as those described by *O'Connor and Hondzo* [2008a] using a Unisense OX-N needle sensor (tip diameter of 1.1 mm) with a PA2000 picoammeter (Unisense, Aarhus, Denmark) sampling at a frequency of 1 Hz. A Rickly point gage (Rickly Hydrological, Columbus, OH) with 1-mm precision was attached to a tripod and used to traverse the needle sensor. Information regarding the Iowa River sampling site is included in the auxiliary material.

[29] The depth zonation of DO production and uptake rates were estimated from the concentration profiles within the sediments using the PROFILE model [*Berg et al.*, 1998]. This model fits concentration data to equation (1) describing one-dimensional, steady state diffusion and includes a statistical algorithm to minimize the number of zones needed to match the measured concentration profile. The DO concentration at the sediment-water interface and a zero flux at a depth below the DO penetration depth (δ, where $C = 0$) were used as boundary conditions for the model. The PROFILE analysis was performed twice for each profile, first using molecular diffusion (D'_m) described by equation (2), and then using effective diffusion (D_e) described by the scaling relationship developed in section 3.2. The net DO flux (J_{DO}) to the sediments was calculated using a sediment-side estimate from the production/uptake zones according to

$$J_{DO} = \int_{i=0}^{\delta} R dy \tag{34}$$

[1] Auxiliary materials are available in the HTML. doi:10.1029/2008WR007160.

Table 2. Summary of Sediment and Fluid-Flow Conditions for Dissolved Oxygen Profile Data Sets

Study	Experiment	d_g (mm)	K (10^{-6} cm^2)	θ	u_* (cm s^{-1})	U (cm s^{-1})	H (cm)
Guss[a] (flume)	E-2	0.4	7.0[b]	0.50	0.21	2.8	3.0
	E-1	0.4	7.0[b]	0.50	0.41	10.5	3.0
	D-2	0.4	7.0[b]	0.50	0.61	23.3	3.0
O'Connor[c] (channel)	OC-1	6.8	2.2	0.35	0.15	1.0	8.0
	OC-2	6.8	1.6	0.35	0.41	5.0	16.0
O'Connor[d] (flume)	2	0.4	2.0	0.60	0.23	4.0	7.5
	5	0.4	2.0	0.60	0.44	8.2	7.5
	6	0.4	2.0	0.60	0.56	11.2	7.5
	10	0.4	2.0	0.60	0.46	9.0	7.5
	11	0.4	2.0	0.60	0.53	11.0	7.5
Iowa River (field)	MP2	25.0[e]	0.7	0.32	4.80	58.3	52.0
	MP4	40.0[e]	0.04	0.32	2.70	27.2	34.5

[a] *Güss* [1998].
[b] Estimated using equation (30).
[c] *O'Connor and Hondzo* [2008a].
[d] *O'Connor and Hondzo* [2008b].
[e] d_{90} values are reported.

where R is the net uptake rate, so a negative value indicates DO production. This estimate of J_{DO} was compared to measured DO fluxes (J_m) that were obtained using water-side flux estimation methods as described in each study, and the method described by *O'Connor and Hondzo* [2008a] was used for the Iowa River data.

4. Results

4.1. Scaling Effective Diffusion Using Hyporheic Exchange Data Sets

[30] The experimental D_e values derived from the hyporheic tracer data were compared to individual variables describing fluid-flow and sediment conditions. The comparisons exhibited positive correlations (Figure 1), and all correlations were statistically significant ($p < 0.05$) except for the correlation with stream depth, H (Figure 1c). No single variable serves as a good predictor for D_e as expected. These individual correlations were used as guidelines in selecting variables for dimensional analysis with the notion that a variable with greater explanatory power individually, will facilitate a better collapse of the experimental D_e data in a multivariate dimensionless expression.

[31] The variables listed in equation (31) for scaling D_e to fluid-flow and sediment characteristics is the final result of the dimensional analysis. Several iterations of the three

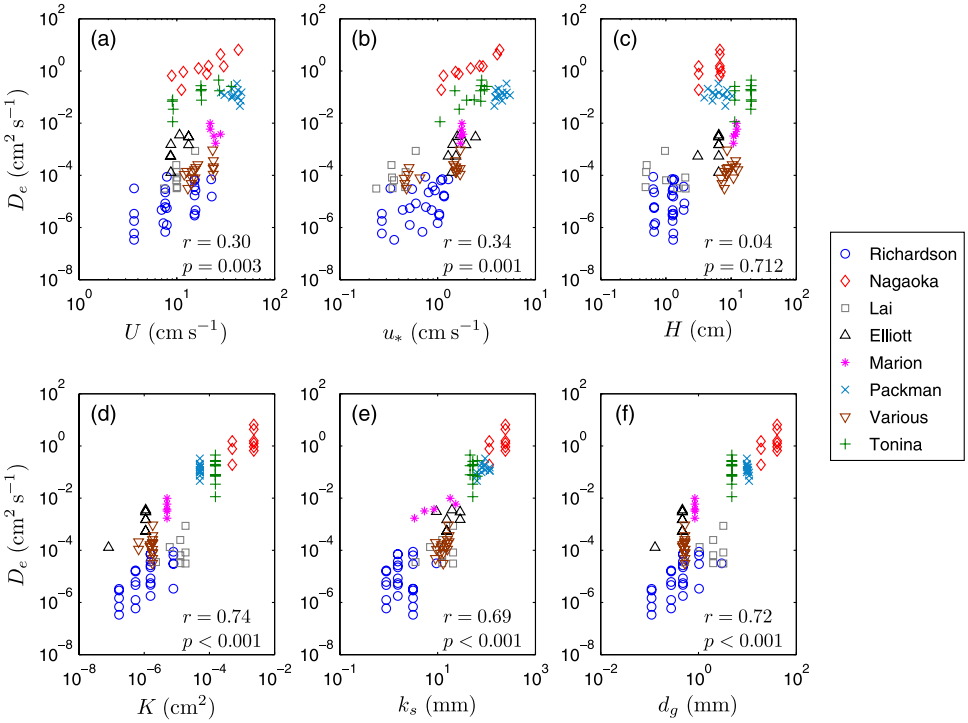

Figure 1. Correlations between effective diffusion values, D_e, and variables describing fluid-flow and sediment conditions: (a) average velocity, U; (b) shear stress velocity, u_*; (c) flow depth, H; (d) permeability, K; (e) roughness height, k_s; and (f) geometric mean particle size, d_g.

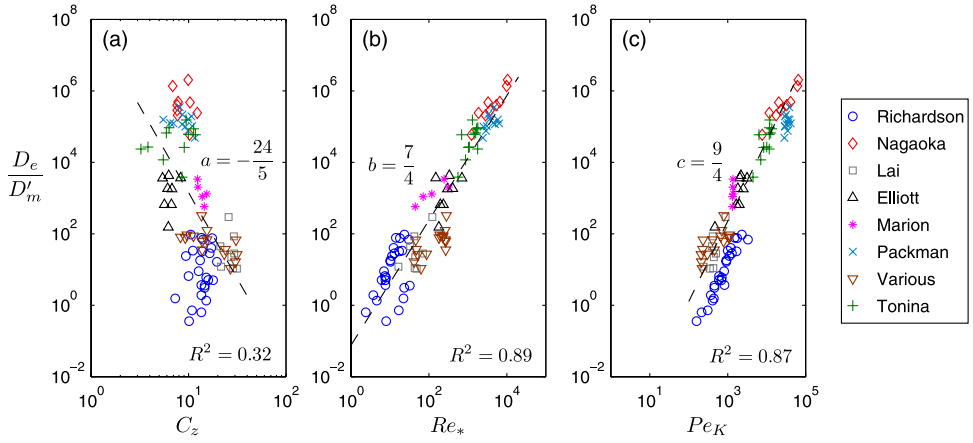

Figure 2. Correlations between the dimensionless effective diffusion, D_e/D'_m, and the dimensionless groupings from equation (33): (a) Chézy coefficient, $C_z = U/u_*$; (b) the shear Reynolds number, $Re_* = u_* k_s/\nu$; and (c) the permeability Péclet number, $Pe_K = u_* \sqrt{K}/\nu$. The scaling coefficients a, b, and c are the slopes of the individual plots.

steps described in section 3.2 were performed, and the variables listed in equation (31) provided the best collapse in the experimental D_e data. Correlations between the dimensionless groups of equation (32) that were used to determine the scaling exponents a, b, and c in equation (33) are shown in Figure 2. Positive correlations were observed for D_e/D'_m with Re_* and Pe_K with similar slopes (~2) and R^2 = 0.89 and 0.87, respectively. The correlation between D_e/D'_m and C_z depicted a negative correlation with a high degree of scatter in the data (R^2 = 0.32) and a slope of approximately −5. This weak correlation with C_z is partially caused by the fact that C_z values only range between 2 and 40 whereas the values for D_e/D'_m range over six orders of magnitude.

[32] The C_z term was dropped from equation (33) because its weak correlation with D_e/D'_m did not provide explanatory power. A plot of D_e/D'_m versus $Re_*^{7/4} Pe_K^{9/4}$ had a slope of 0.55, which was combined with the scaling exponents b = 7/4 and c = 9/4 to give the final D_e scaling equation as

$$\frac{D_e}{D'_m} = \begin{cases} 5 \times 10^{-4} Re_* Pe_K^{6/5} & \text{for } Re_* Pe_K^{6/5} \geq 2000 \\ 1 & \text{for } Re_* Pe_K^{6/5} < 2000. \end{cases} \quad (35)$$

where the inverse of the scaling constant ($\alpha = 5 \times 10^{-4}$) provided a threshold value in transport conditions ($Re_* Pe_K^{6/5}$ = 2000) below which transport was governed by molecular diffusion resulting in $D_e/D'_m = 1$ (Figure 3). All but one of the experimental D_e data points were above the threshold condition for molecular diffusion. The scaling relationship described by equation (35) had a slope of one and explained 95% of the variance with 95% confidence intervals of the slope between 0.93 to 1.02, and α between 2.4×10^{-4} and 1×10^{-3}.

[33] The experimental tracer D_e data was compared with the estimation expressions using the pumping model, slip flow model, and the scaling relationship described by equations (22), (27), and (35), respectively (Figure 4). The pumping model estimation is a function of h_m, which implies the presence of bed forms. For flat bed experiments, Δ was assumed to be d_g in equation (14). The estimation expression of the slip flow model requires a normalized slip velocity, u_s^+. None of the hyporheic exchange investigations provided depth profiles of the streamwise velocity, so the method used by *Fries* [2007] could not be used. Instead, we used the expression of *Engelund* [1970], $u_s^+ = 1.9 + 2.5 \ln(H/k'_s)$ where $k'_s = 2.5 d_g$ is the equivalent sand roughness height, which resulted in u_s values that ranged between $3-15 \cdot u_*$. The pumping model estimation matched experimental D_e values for the experiments of *Elliott and Brooks* [1997b], *Marion et al.* [2002], and *Packman et al.* [2004], but overestimated D_e for the other studies (Figure 4a). The slip flow model underestimated experimental D_e values for all the studies examined.

4.2. Effective Diffusion Model for Interpreting Dissolved Oxygen Uptake

[34] The DO concentration profiles listed in Table 2 were analyzed using the effective diffusion model (D_e, equation (35)) and the traditional molecular diffusion model (D'_m, equation (2)). The PROFILE model was used to determine the depth distribution of the net DO uptake rate (R in equation (1)). Experiment D-2 from *Güss* [1998] depicted a different pattern in the distribution of R between the molecular and effective diffusion models (D_e/D'_m = 3.5), yet both models matched the DO concentration profile. For molecular diffusion, R = 118 g m^{-2} d^{-1} from the sediment-water interface down to 1.3 mm, whereas the effective diffusion model had R = 0 down to 0.6 mm and R = 950 g m^{-2} d^{-1} between 0.6 and 1.3 mm (Figure 5a). Experiment 6 from *O'Connor and Hondzo* [2008b] demonstrated similar patterns in the distribution of R between molecular and effective diffusion models but with varying rates. From the sediment-water interface down to 0.8 mm, R increased from 555 to 1040 g m^{-2} d^{-1} (Figure 5b).

[35] The DO profiles from the experiments by *Güss* [1998] and *O'Connor and Hondzo* [2008b] were measured in flumes that prevented light penetration, which inhibited photosynthesis. For the experiments of [*O'Connor and Hondzo*, 2008a] and the Iowa River, the DO concentration profiles were performed in sediments with algal presence, so DO production was a factor. The molecular and effective diffusion models produced similar patterns in the distribu-

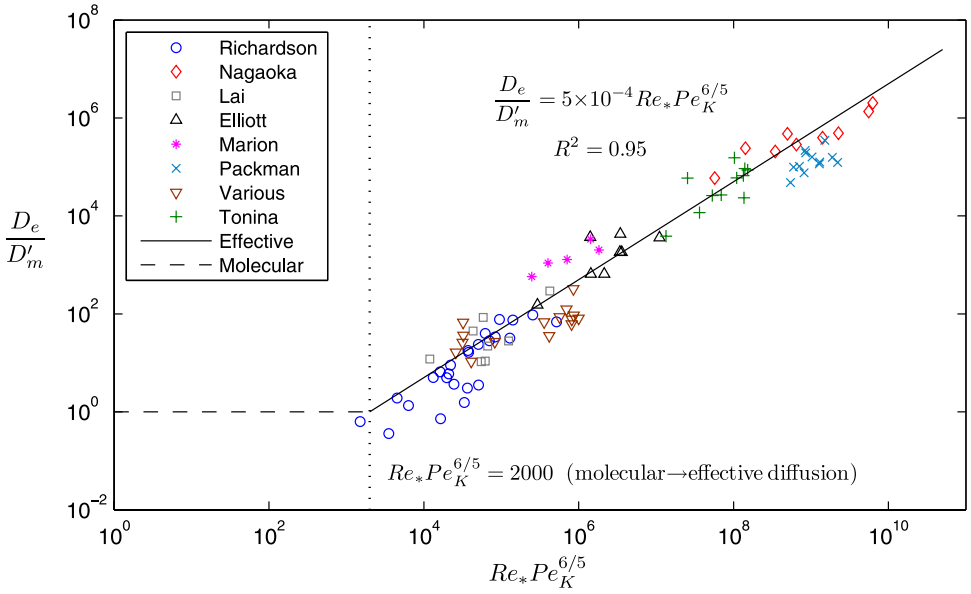

Figure 3. Resulting scaling relationship of the effective diffusion coefficient, D_e, from dimensional analysis. The change from molecular based diffusion described by equation (2) to effective diffusion described by equation (35) occurs at the threshold value of $Re_* Pe_K^{6/5} = 2000$.

tion of DO uptake and production, but with large differences between rates (Figure 6). Experiment OC-2 from [*O'Connor and Hondzo*, 2008a] demonstrated DO production from the sediment-water interface down to 0.85 mm with $R = -184$ and -1.2×10^4 g m^{-2} d^{-1} for the molecular and effective diffusion models, respectively. Below the DO production zone, DO uptake rates were slightly greater between $R = 204$ and 1.3×10^4 g m^{-2} d^{-1} down to 1.7 mm in the sediments. The DO uptake rates then decreased to $R = 5$ and 318 g m^{-2} d^{-1} down to the DO penetration depth ($\delta = 4.25$ mm, Figures 6a and 6b). A similar pattern of a sharp transition between DO production

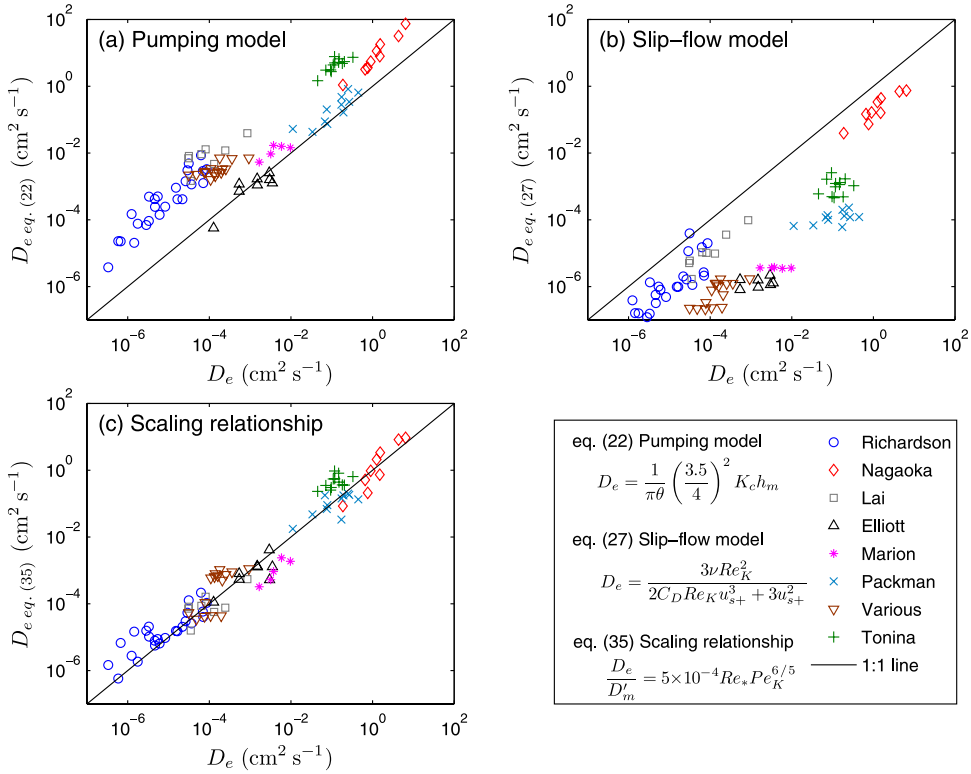

Figure 4. Comparison between experimentally derived effective diffusion values, D_e, and estimates based on the (a) pumping model, (b) slip flow model, and (c) scaling relationship described by equations (22), (27), and (35), respectively.

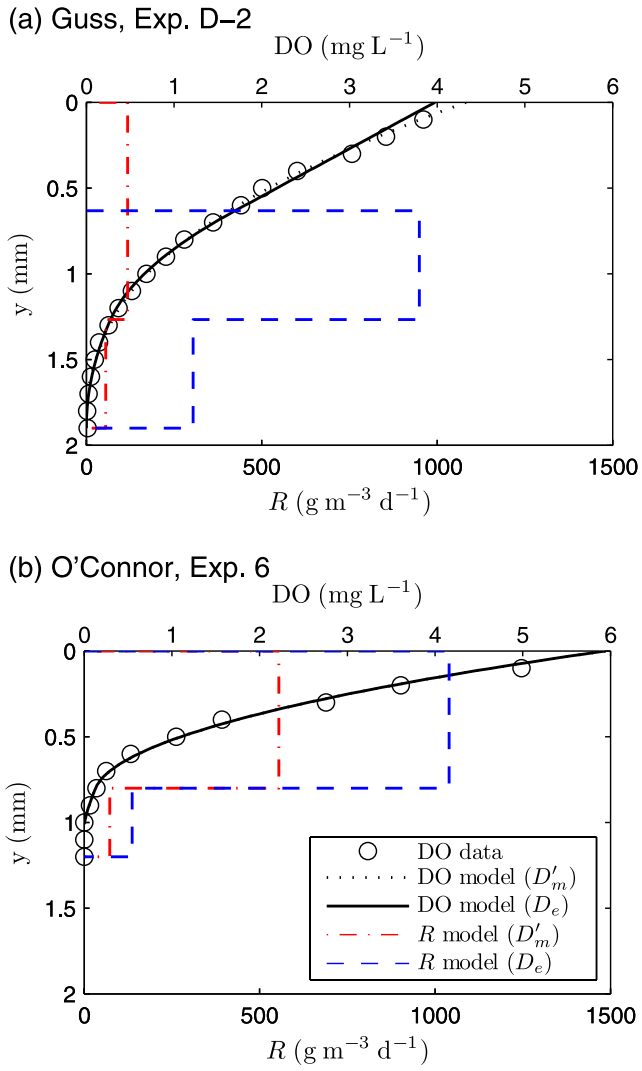

Figure 5. Depth distribution of measured dissolved oxygen (DO) concentrations, as well as modeled concentrations and uptake rates, R, for (a) experiment D-2 from *Güss* [1998] and (b) experiment 6 from *O'Connor and Hondzo* [2008b]. The DO concentration and uptake profiles were modeled using both molecular diffusion, D'_m, and effective diffusion, D_e.

and uptake was observed for experiment MP2 for the Iowa River study. However, the maximum DO production was located 6 mm below the sediment-water interface with $R = -4.1$ and -4.8×10^4 g m^{-2} d^{-1} for the molecular and effective diffusion models. The maximum DO uptake was slightly lower than the maximum DO production with $R = 3.8$ and 4.4×10^4 g m^{-2} d^{-1} from 12 to 18 mm within the sediments, followed by $R = 0.8$ and 1.6×10^4 g m^{-2} d^{-1} down to $\delta = 24$ mm (Figures 6c and 6d).

[36] The differences in DO uptake and production between the effective and molecular diffusion models (Figures 5 and 6) demonstrates a range in D_e/D'_m values between 1 and 3750 for all the studies examined. The net DO flux for the molecular and effective diffusion models, estimated by the integration of the DO uptake profiles (J_{DO}, equation (34)), was compared to an independent measurement of the flux (J_m) for each experiment (Table 3), with the ratio of the fluxes shown in Figure 7. For the experiments of *Güss* [1998], both the effective and molecular diffusion models underestimated J_m, except for the effective diffusion model in experiment D-2, which closely matched J_m. For experiments 5, 6, 10, and 11 of *O'Connor and Hondzo* [2008b] the measured J_m values were between the molecular and effective diffusion model fluxes, yet the effective diffusion model provided better flux estimates based on percent difference. In general, for $D_e/D'_m < 3$, the molecular and effective diffusion models bounded the measured flux while for $D_e/D'_m \geq 3$, the effective diffusion model closely match the measured flux and the molecular model underestimated the flux by as much as a factor of 10^5 for $D_e/D'_m = 3750$.

5. Discussion

[37] Studying biogeochemical reactions in aquatic sediments is challenging because of the complexity of the individual physical, chemical, and biological components. The complexity is one reason why numerical modeling approaches are becoming a popular tool for addressing coupled biogeochemical-hyporheic processes [e.g., *Meysman et al.*, 2007]. However, measurements of hyporheic exchange and biogeochemical gradients need to be continued because simple kinetic expressions used for modeling studies are not directly transferable to systems with complex sediments where multiple controlling factors such as redox potential, organic carbon, microbiological gradients, and coupled biogeochemical processes all interact with transport processes to control reaction rates. Quantifying biogeochemical reaction rates on the basis of measured concentration profiles provides a method for examining the depth distribution of the process in relation to gradients of controlling environmental factors in the sediments. This empirical approach requires lots of data collection to capture the inherent spatial and temporal variability in controlling factors. The data collected could be used for quantifying biogeochemical reaction rates in a similar manner that was applied to quantifying hyporheic exchange in this study, through the development of scaling relationships between the reaction rates and controlling environmental factors, for which some progress has been made [e.g., *O'Connor et al.*, 2006]. However, further work is needed in identifying all relevant variables affecting the individual biogeochemical reactions and determining the appropriate methods for their quantification.

[38] Measurements of biogeochemical gradients of interest are relatively simple to obtain (e.g., microsensors and pore water samplers), and the D_e scaling relationship developed in this study can be used to infer reaction rates across a wide range in sediment and fluid-flow conditions. This tool will allow researchers to address several of the key questions regarding the complex interactions among controlling factors, such as the debate over organic matter quality versus transport control on carbon cycling in sediments [e.g., *Rothman and Forney*, 2007; *Boudreau et al.*, 2008], as well as extend research on coupled biogeochemical processes, like DO uptake and denitrification [e.g., *Arnon et al.*, 2007; *O'Connor and Hondzo*, 2008b] in systems with more complex transport conditions. The examples of DO uptake rates based on scaled D_e transport values presented in this study were all under steady state conditions; however, this type of analysis could be extended

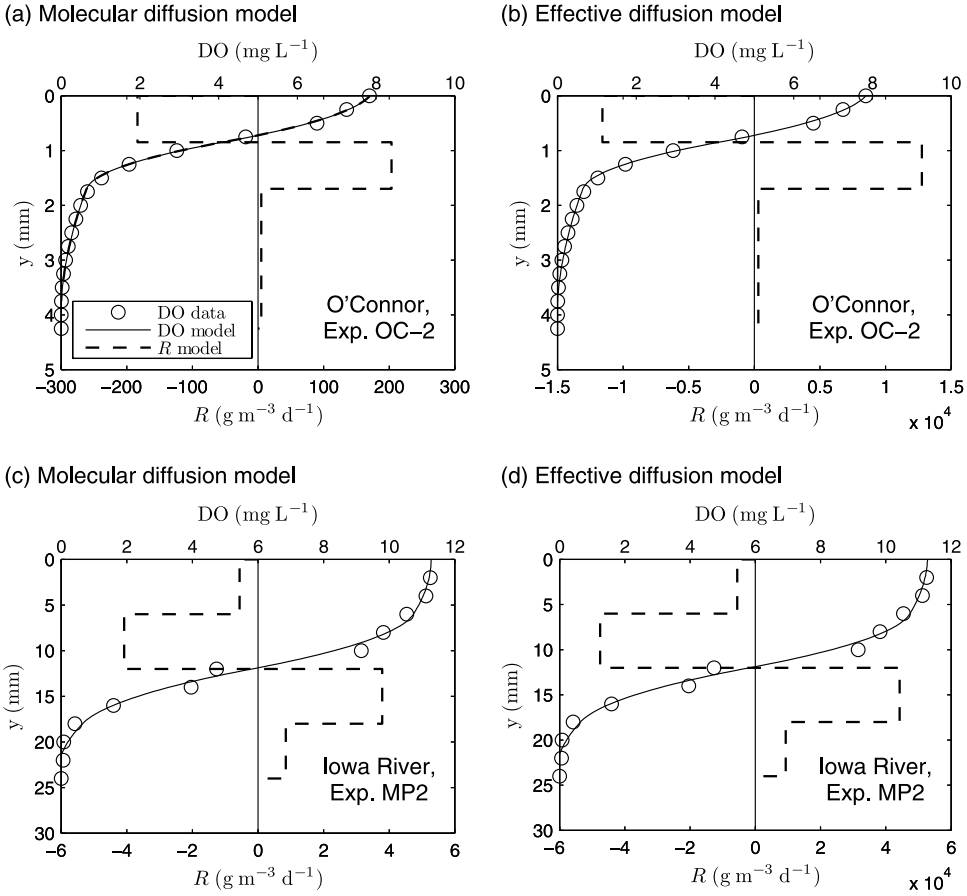

Figure 6. Depth distribution of measured dissolved oxygen (DO) concentrations, as well as modeled concentrations and uptake rates, R, using both the molecular (D'_m) and effective (D_e) diffusion models for (a and b) experiment OC-2 from *O'Connor and Hondzo* [2008a] and (c and d) site MP2 from the Iowa River study. Note the change in the x axis scale between the molecular and effective models.

to address nonsteady processes as well. For example, photosynthesis rates are controlled by solar radiation that varies over the course of the day. Typically, DO concentration profiles can be obtained on the order of minutes, so multiple profiles can be measured to address the nonsteady nature of photosynthesis. The value of D_e used to interpret these profiles will be steady over time scales where the individual sediment and fluid-flow variables defining D_e are steady.

[39] Accurately quantifying the transport in aquatic sediments is essential to this approach for obtaining biogeochemical reaction rates. As was shown in this study, the DO

Table 3. Comparison of Molecular (D'_m) and Effective (D_e) Diffusion Models With the Measured Dissolved Oxygen Flux (J_m)

Study	Experiment	D_e/D'_m	J_{DO} (D'_m) (g m^{-2} d^{-1})	J_{DO} (D_e) (g m^{-2} d^{-1})	J_m (g m^{-2} d^{-1})
Guss (flume)	E-2	1	0.114	0.114	0.658[a]
	E-1	1.5	0.156	0.281	0.666[a]
	D-2	3.5	0.185	0.794	0.733[a]
O'Connor (channel)	OC-1	3	0.028	0.230	0.290[b]
	OC-2	25	0.030	1.830	1.858[b]
O'Connor (flume)	2	1	0.340	0.340	0.353[c]
	5	1.2	0.338	0.541	0.441[c]
	6	2.1	0.473	0.864	0.577[c]
	10	1.2	0.558	0.892	0.839[c]
	11	1.6	0.744	1.172	0.996[c]
Iowa River (field)	MP2	3750	3.96×10^{-5}	2.904	2.905[b]
	MP4	304	2.21×10^{-3}	2.098	2.982[b]

[a]Calculated from dispersion model described by *Güss* [1998].
[b]Calculated from similarity model described by *O'Connor and Hondzo* [2008a].
[c]Calculated using a mass balance described by *O'Connor and Hondzo* [2008b].

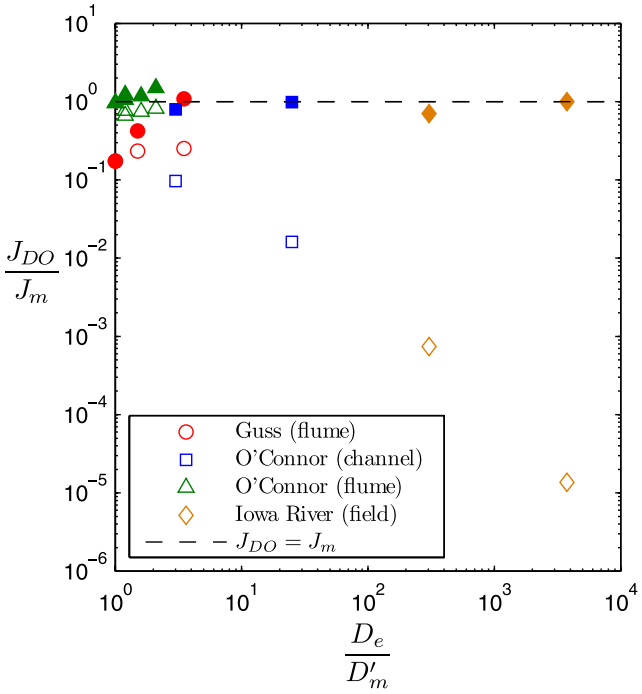

Figure 7. Comparison of the PROFILE model estimate of DO flux, J_{DO}, using equation (34) to the measured flux, J_m, using molecular diffusion (D'_m, open symbols) and effective diffusion (D_e, closed symbols).

uptake rates followed the same depth distribution pattern between molecular and effective diffusion models, but with substantial differences in the DO uptake rates (Figures 5 and 6). The transport was verified by comparing DO flux estimates using equation (34) with measured flux values. An additional check on the accuracy of the scaled D_e transport term could be obtained by examining multicomponent profiles (e.g., combined DO and nitrate concentration profiles) where the D_e value should be similar (only a small difference in D'_m values affecting the value of D_e) and the interpreted uptake rates can be compared to measured surface fluxes for each component. Additionally, the D_e scaling relationship developed in this study was based on flume tracer experiments, which can be improved upon by further advancements in measuring transport in aquatic sediments, such as the use of ultrasonic velocity profiler (UVP) technology [*Manes et al.*, 2006].

5.1. Flow and Sediment Variables Important to Hyporheic Exchange

[40] The first step in developing a scaling relationship for D_e was to determine the characteristic velocity and length scales that best predict hyporheic exchange over a wide range in conditions. To the best of our knowledge, the combined hyporheic exchange data set used in this study is the most comprehensive data set assembled to date in terms of the ranges in individual sediment and fluid-flow variables (Table 1). Figure 1 shows the correlation between measured D_e values and individual variables describing fluid-flow and sediment conditions. Previous scaling attempts using relatively limited data sets by *Packman and Salehin* [2003] and *Packman et al.* [2004] used the variables U, d_g, and H to scale D_e, whereas *Richardson and Parr* [1988] used the variables u_* and K. The compiled data set used in this study showed that u_* was slightly better than U at predicting D_e, and that k_s, K, and d_g had stronger correlations with D_e than H (Figure 1).

[41] The final D_e scaling relationship (equation (35)) includes the transport term $Re_* Pe_K^{6/5}$ depicted by the x axis of Figure 3. The 6/5 exponent on Pe_K is a result of fitting experimental D_e data using dimensional analysis, but is very close to a value of one. Using this approximation $D_e \sim Re_* Pe_K$ implies that

$$D_e \sim u_*^2, k_s(d_{90}, \Delta, \lambda), \nu^{-1}, \sqrt{K}, D'_m(D_m, \theta) \qquad (36)$$

which has similar features to the previous scaling attempts by *Richardson and Parr* [1988], *Packman and Salehin* [2003], and *Packman et al.* [2004]. However, the scaling relationship developed in this study correctly compares effective to molecular diffusion in the sediments by including the effects of tortuosity, as well as including a means to collapse data between flat bed and bed form geometries. The use of k_s and D'_m introduces empiricism into the dimensional analysis through equations (2) and (29). However, these terms also allow for the relatively simple scaling relationship (equation (35)) to include the effects of θ, Δ, λ, and d_{90} that are variables known to affect hyporheic exchange. In the end, the resulting D_e scaling relationship explained 95% of the variance in the comprehensive data set, over a wide range in fluid-flow and sediment conditions. This high degree of predictive power indicates that the key transport mechanisms were represented by the variables chosen and the formulation of the D_e scaling relationship.

5.2. Transport Mechanisms Involved With Hyporheic Exchange

[42] Quantifying hyporheic exchange in natural systems is complicated by the many transport mechanism involved. The pumping and slip flow model assume advective transport governed by Darcy's law in the sediment. The difference between the two models is the driving force at the sediment-water interface, where the pumping model focuses on pressure (head distributions) and the slip flow model on shear (velocity distributions). However, both models do not account for molecular diffusion and turbulent transport that limits their applicability across a broad range of fluid-flow and sediment conditions.

[43] Figure 4 compares the pumping, slip flow, and effective diffusion models in their prediction of measured D_e values. The pumping model estimate of D_e assumes a sinusoidal head distribution at the sediment-water interface, which is why it worked well for experiments with regularly spaced bed forms. The experiments of *Richardson and Parr* [1988] and *Lai et al.* [1994] were performed using flat beds with particle sizes <3 mm. The pumping model overestimated D_e for these experiments because it is unlikely that the smooth beds generated substantial pressure gradients at the interface, so the flux was dominated by momentum flux induced by shear. For the experiments of *Nagaoka and Ohgaki* [1990] and *Tonina and Buffington* [2007], the overestimation of D_e was caused by the large particle sizes and irregular bed forms (large λ relative to Δ values) that created a nonsinusoidal head distribution at the interface. Its

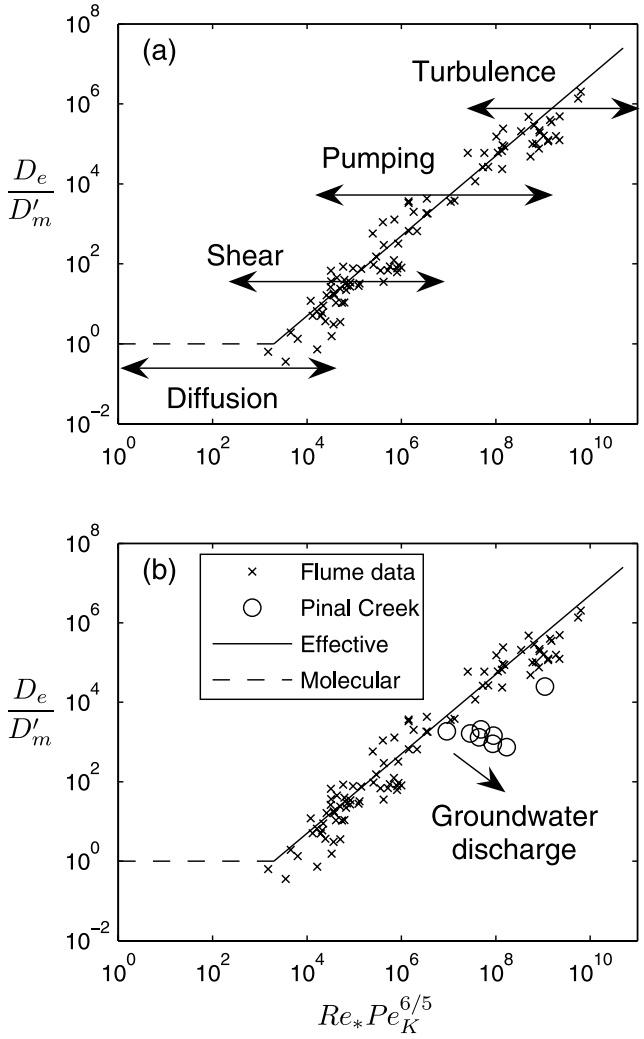

Figure 8. (a) Ranges in transport conditions (fluid-flow and sediment characteristics represented by $Re_* Pe_K^{6/5}$) for the various mechanisms involved with hyporheic exchange. (b) Comparison between effective diffusion scaling relationship based on the combined flume data sets and field tracer data from Pinal Creek, AZ [*Harvey and Fuller*, 1998; *Fuller and Harvey*, 2000]. Pinal Creek had large groundwater inputs that limited hyporheic exchange.

not clear why the pumping model overestimated D_e for the studies of the "Various" investigations as they had similar experimental characteristics as those given by *Elliott and Brooks* [1997b], with exception of a lower range in u_* values (Table 1).

[44] The slip flow model underestimated measured D_e values because the *Engelund* [1970] expression for u_s^+ generated slip velocities at the sediment-water interface that were $3-15 \cdot u_*$, which are very unlikely. This analysis is still valuable in assessing the role of the slip flow model on hyporheic exchange. The flat bed experiments of *Richardson and Parr* [1988] and *Lai et al.* [1994] closely matched measured D_e values if u_s^+ was reduced by a factor of 3, but all other studies were still underestimated. The slip flow model assumes that transport is dominated by shear forces across the interface, which occurs over a smooth boundary. A simple calculation of the dimensionless hydraulic roughness height ($k_s^+ = d_g u_* / \nu$) resulted in hydraulically smooth bed conditions ($k_s^+ < 5$ [*Nezu and Nakagawa*, 1993]) for the experiments of *Richardson and Parr* [1988] and *Lai et al.* [1994], as well as a few of the experimental runs with bed forms in the studies of *Elliott and Brooks* [1997b] and of the "Various" investigations. This suggests that shear-induced hyporheic exchange is relevant for hydraulically smooth flat beds, but for conditions with larger particle sizes and bed forms there are pressures forces generated at the sediment-water interface that dominate over shear-induced momentum flux.

[45] Experimental conditions that produced good agreement between modeled and measured D_e values in Figure 4 can be used to assess ranges in fluid-flow and sediment conditions that are relevant to molecular diffusion, shear-induced flow, advective pumping, and turbulence penetration. Figure 8a depicts the qualitative ranges in sediment and fluid-flow conditions (represented as $Re_* Pe_K^{6/5}$) for the mechanisms involved with hyporheic exchange. Molecular diffusion dominates transport between $10^0 < Re_* Pe_K^{6/5} < 1.4 \times 10^4$, followed by overlapping regions consisting of shear-induced flow between $10^3 < Re_* Pe_K^{6/5} < 2 \times 10^6$, advective pumping between $3 \times 10^5 < Re_* Pe_K^{6/5} < 1.6 \times 10^9$, and turbulence penetration for $Re_* Pe_K^{6/5} > 1.3 \times 10^7$. This analysis shows that for a given set of transport conditions, there are multiple exchange processes involved, which agrees with the conclusion of *Packman and Salehin* [2003] for why using an effective diffusion model is appropriate.

5.3. Hyporheic Scaling Relationship for Field Investigations

[46] There are two main factors that need to be considered for applying the developed scaling relationship for assessing hyporheic exchange in the field: groundwater discharge and scale. For the flume experiments used to develop the scaling relationship of D_e, solute flux was controlled by physical forcing from the overlying flow. However, in natural streams, physical forcing on hyporheic exchange can also occur on the sediment-side of the domain from discharging groundwater [*Woessner*, 2000]. The effect of discharging groundwater on hyporheic exchange can be viewed as the "underflow" component in the advective pumping model, which was shown to reduce the net mass exchange [*Elliott and Brooks*, 1997a]. In this study, we examined the effect of groundwater discharge in relation to the scaling relationship for D_e using nested piezometer data from tracer studies conducted at Pinal Creek (located in central Arizona), which was characterized by unusually high groundwater discharge rates for a small stream [*Harvey and Fuller*, 1998; *Fuller and Harvey*, 2000]. The tracer-based values of D_e measured in Pinal Creek fall slightly below the line of the scaling relationship, as shown in Figure 8b. This is the result of groundwater discharge generating a physical limitation of hyporheic exchange, which is not represented in the variables incorporated into the scaling relationship.

[47] The flume investigations used to develop the pumping, slip flow, and scaling relationship models of hyporheic exchange used a wide range in fluid-flow and sediment characteristics, but for each experiment the transport variables were fairly uniform. Thus the application of these

hyporheic exchange models should be considered relevant at the patch scale. We use the term patch scale to indicate that the hyporheic exchange models are relevant for scales over which variables describing transport such as u_*, k_s, and K can be considered characteristic. Natural streams consist of geomorphic features such as pools, riffles, and meanders that generate heterogeneity in variables describing bed geometry, fluid-flow, and sediment characteristics. In order to apply hyporheic exchange models to field investigations, the issue of scale in the controlling fluid-flow and sediment variables must be considered.

[48] The dimensional analysis used in this study generated the dimensionless terms C_z, Re_*, and Pe_K, which are qualitatively known to affect hyporheic exchange as they describe flow resistance, as well as advective and diffusive transport processes. The weak correlation between D_e and C_z ($R^2 = 0.32$) was surprising, but also indicates the scale dependency for hyporheic exchange models. For reach-scale tracer measurements of transient storage, the Darcy-Weisbach friction factor ($f = 8gHS/U^2$) has been shown to be a good predictor for reach-averaged hyporheic exchange [e.g., *Harvey et al.*, 2003; *Zarnetske et al.*, 2007]. Mathematically f and C_z are similar ($C_z = \sqrt{8/f}$) if uniform flow is assumed in the channel. So, while flow resistance quantified as a friction factor appears to explain hyporheic exchange at the reach scale, it does not factor into the transport mechanisms incorporated into the patch-scale hyporheic models.

5.4. Interpretation of Dissolved Oxygen Uptake Rates

[49] Our main purpose for quantifying hyporheic exchange as an effective diffusion process was to interpret biogeochemical reaction rates from concentration profiles in systems with complex fluid-flow and sediment conditions. DO uptake and production occurs in near-surface sediments and is controlled by oxidation, respiration, decomposition, and photosynthesis, for which the complex interaction of these processes can be represented as zero-order kinetics like the R term in equation (1) [*DiToro*, 2001]. Examining the differences between the molecular and effective diffusion models for interpreting DO concentration profiles demonstrated large differences in net uptake rates (Figures 5 and 6). With exception to the DO profile of experiment D-2 of *Güss* [1998], the depth zonation of DO uptake and production did not change between the molecular and effective diffusion models, only the magnitude of the volumetric uptake and production rates changed.

[50] The experiments of *Güss* [1998] and *O'Connor and Hondzo* [2008b] were done in shaded flumes, so photosynthesis was inhibited. The values of R were largest directly below the sediment-water interface except for the effective diffusion model of experiment D-2 of *Güss* [1998], which depicts transport dominating over DO uptake down to 0.6 mm (Figure 5). This interpretation implies that the DO flux to the sediments exceeded the intrinsic DO uptake capability of the sediment, which is attributable to the transition between water- to sediment-side control of the net DO flux. The experiments of *O'Connor and Hondzo* [2008a] and those performed in the Iowa River occurred in sediments with algae, so photosynthesis was a factor on the DO dynamics. DO production occurred directly below the sediment-water interface and there was a sharp transition between the maximum DO production and DO uptake zones (Figure 6). This suggests that the DO production in the surface layer sediments stimulates DO uptake in the sediments below, which is consistent with the findings of algal-induced respiration hot spots described by *Jones et al.* [1995].

[51] The accuracy of the molecular and effective diffusion models interpretation of the sediment DO concentration profiles was checked by calculating the net DO flux using equation (34) and comparing it to a measured flux (J_m). The methods used to calculate J_m varied between experiments, but all of them used a water-side method of determining flux, which have been traditionally favored over sediment-side approaches like equation (34) because of the difficulty of quantifying the transport in porous sediments [*Gundersen and Jørgensen*, 1990]. For $D_e/D'_m \geq 3$, the effective diffusion model closely matched the measured flux while the molecular diffusion model greatly underestimated the measured flux (Figure 7). Matching water-side flux values gives confidence in the ability of the effective diffusion model for interpreting biogeochemical profiles. While several studies have examined the importance of the zonation of uptake and production rates on biogeochemical reactions under molecular diffusion transport [e.g., *Revsbech et al.*, 2005], the results of this study demonstrated that the location of the reaction zones did not change between molecular and effective diffusion models, but the reaction rates were increased by several orders of magnitude. Therefore, using the proposed D_e scaling relationship for interpreting the zonation of biogeochemical reactions can provide an accurate depiction of the net biogeochemical reaction rates in ecosystems with complex transport mechanisms.

6. Summary

[52] Hyporheic exchange is a result of many transport mechanisms over a range in fluid-flow and sediment conditions. The scaling relationship for D_e developed in this study is an empirical model that retains features of the developed theories regarding hyporheic exchange. This effective diffusion representation of hyporheic exchange is directly compatible with models used to interpret biogeochemical reaction rates on the basis of chemical profiles across the sediment-water interface. Comparisons between modeled and measured DO fluxes from a variety of systems presented in this study show good agreement over a wide range in fluid-flow and sediment conditions. Applying hyporheic exchange models to complex natural systems needs to address factors relating to variability in the controlling fluid-flow and sediment characteristics, as well as the potential for resistance to hyporheic exchange within the sediments (e.g., groundwater discharge). The scaling approach used in this study can be easily adapted to include groundwater discharge and other factors affecting hyporheic exchange once experimental evidence becomes available that can be incorporated into dimensional analysis. This empirical approach of examining hyporheic exchange and biogeochemical reactions serves as a methodology that can be used to study the coupling of these processes in complex natural systems. Future work addressing theoretical advancements, on either the hyporheic exchange or the biogeochem-

istry, can benefit from using a scaling approach as a means to examine the key variables and processes involved.

Notation

a, b, c scaling exponents.
A_s surface area of sediment bed (L^2).
C solute concentration (ML^{-3}).
C_D Forchheimer form drag coefficient.
C_z Chézy resistance coefficient (U/u_*).
C_o initial solute concentration (ML^{-3}).
$C_{o,s}$ initial saturated bed concentration (ML^{-3}).
C_w water solute concentration (ML^{-3}).
C^* normalized concentration (C/C_o).
D_b biodiffusivity ($L^2\ T^{-1}$).
D_d dispersion ($L^2\ T^{-1}$).
D_e effective diffusion ($L^2\ T^{-1}$).
D_m molecular diffusion ($L^2\ T^{-1}$).
D'_m sediment molecular diffusion (βD_m) ($L^2\ T^{-1}$).
d_g geometric mean particle size (L).
d_{90} particle size for which 90% of sediment is finer (L).
F_b net body force (MLT^{-2}).
f Darcy-Weisbach friction factor.
H stream depth (L).
h piezometric head (L).
h_m piezometric head at sediment surface (L).
J solute flux ($ML^{-2}\ T^{-1}$).
J_{DO} DO flux, equation (34) ($ML^{-2}\ T^{-1}$).
J_m measured DO flux ($ML^{-2}\ T^{-1}$).
K permeability (L^2).
K_c hydraulic conductivity (LT^{-1}).
k_s roughness height (L).
k'_s equivalent sand roughness (L).
k_s^+ hydraulic roughness height ($d_g u_*/\nu$).
M mass accumulation in bed (ML^{-2}).
M_w mass accumulation in water (ML^{-2}).
M' effective penetration depth (M/C_o) (L).
$\mathbf{n}$ unit vector normal to bed.
p pressure ($ML^{-1}\ T^{-2}$).
Pe_K permeability Péclet number ($u_*\sqrt{K}/D'_m$).
Pe_* shear Péclet number ($u_* k_s/D'_m$).
$\overline{q}$ normalized solute flux (LT^{-1}).
R net uptake rate ($ML^{-3}\ T^{-1}$).
$\overline{R}$ residence time function.
Re Reynolds number (UH/ν).
Re_K permeability Reynolds number ($u_*\sqrt{K}/\nu$).
Re_* shear Reynolds number ($u_* k_s/\nu$).
S bed slope.
t time (T).
U average velocity (LT^{-1}).
u_s slip velocity (LT^{-1}).
u_s^+ normalized slip velocity (u_s/u_*).
u_* shear stress velocity (LT^{-1}).
$\mathbf{u}$ velocity vector (LT^{-1}).
V_w water volume, flume experiments (L^3).
$\mathbf{v}$ seepage velocity vector (LT^{-1}).
x streamwise coordinate.
y vertical coordinate.
α dimensionless scaling constant.
β sediment diffusion correction term.
γ empirical constant for equation (14).
Δ bed form height (L).
δ DO penetration depth (L).
θ porosity.
λ bed form wavelength (L).
ν kinematic viscosity ($L^2\ T^{-1}$).
ν_e effective viscosity ($L^2\ T^{-1}$).
ξ time lag (T).
ρ water density (ML^{-3}).

[53] **Acknowledgments.** This research was performed while the first author held a National Research Council Research Associateship at the U.S. Geological Survey in Reston, Virginia. Funding was provided through the National Water Quality Assessment (NAWQA) and National Research Programs of the USGS. Additional support for J. W. H. was provided by the National Science Foundation through award EAR0408744. Field assistance was provided by Dan Nowacki, Lauren McPhillips, and Leanna Westfall for the data collected from the Iowa River. Earlier versions of the manuscript were improved thanks to comments from colleague reviewers Ken Bencala and Heinz Stefan, as well as journal reviewers Bernard Boudreau, Aaron Packman, and two anonymous reviewers. Any use of trade, firm, or product names is for descriptive purposes only and does not imply endorsement by the U.S. Government.

References

Archie, G. E. (1942), The electrical resistivity log as an aid in determining some reservoir characteristics, *Trans. Am. Inst. Min. Metall. Pet. Eng.*, *146*, 54–62.

Arnon, S., K. A. Gray, and A. I. Packman (2007), Biophysical process coupling controls nitrate use by benthic biofilms, *Limnol. Oceanogr.*, *52*, 1665–1671.

Basu, A. J., and A. Khalili (1999), Computation of flow through a fluid-sediment interface in a benthic chamber, *Phys. Fluids*, *11*, 1395–1405.

Beavers, G. S., and D. D. Joseph (1967), Boundary conditions at a naturally permeable wall, *J. Fluid Mech.*, *30*, 197–207.

Berg, P., N. Risgaard-Petersen, and S. Rysgaard (1998), Interpretation of measured concentration profiles in sediment pore water, *Limnol. Oceanogr.*, *43*, 1500–1510.

Berner, R. A. (1980), *Early Diagenesis: A Theoretical Approach*, Princeton Univ. Press, Princeton, N. J.

Boudreau, B. P. (1984), On the equivalence of nonlocal and radial diffusion models for porewater irrigation, *J. Mar. Res.*, *42*, 731–735.

Boudreau, B. P. (1996), The diffusive tortuosity of fine-grained unlithified sediments, *Geochim. Cosmochim. Acta*, *60*, 3139–3142.

Boudreau, B. P., C. Arnosti, B. B. Jørgensen, and D. E. Canfield (2008), Comment on "Physical model for the decay and preservation of marine orgainc carbon," *Science*, *319*, 1616b.

Bouldin, D. (1968), Models for describing the diffusion of oxygen and other mobile constituents across the mud-water interface, *J. Ecol.*, *56*, 77–87.

Cardenas, M. B., and J. L. Wilson (2007), Dunes, turbulent eddies, and interfacial exchange with permeable sediments, *Water Resour. Res.*, *43*, W08412, doi:10.1029/2006WR005787.

Crank, J. (1975), *The Mathematics of Diffusion*, 2nd ed., Oxford Univ. Press, Oxford, U. K.

Dade, W. B., A. J. Hogg, and B. P. Boudreau (2001), Physics of flow above the sediment-water interface, in *The Benthic Boundary Layer: Transport Processes and Biogeochemistry*, edited by B. P. Boudreau and B. B. Jørgensen, chap. 2, pp. 4–43, Oxford Univ. Press, London.

DiToro, D. M. (2001), *Sediment Flux Modeling*, John Wiley, New York.

Elliott, A. H. (1990), Transfer of solutes into and out of streambeds, *Tech. Rep. KH-R-52*, Calif. Inst. of Technol., Pasadena, Calif.

Elliott, A. H., and N. H. Brooks (1997a), Transfer of nonsorbing solutes to a streambed with bedforms: Theory, *Water Resour. Res.*, *33*, 123–136.

Elliott, A. H., and N. H. Brooks (1997b), Transfer of nonsorbing solutes to a streambed with bedforms: Laboratory experiments, *Water Resour. Res.*, *33*, 137–151.

Engelund, F. (1970), Instability of erodible beds, *J. Fluid Mech.*, *42*, 225–244.

Findlay, S. (1995), Importance of surface-subsurface exchange in stream ecosystems: The hyporheic zone, *Limnol. Oceanogr.*, *40*, 159–164.

Freeze, R. A., and J. A. Cherry (1979), *Groundwater*, Prentice-Hall, Englewood Cliffs, N. J.

Fries, J. S. (2007), Predicting interfacial diffusion coefficients for fluxes across the sediment-water interface, *J. Hydraul. Eng.*, *133*, 267–272.

Fuller, C. C., and J. W. Harvey (2000), Reactive uptake of trace metals in the hyporheic zone of a mining-contaminated stream, Pinal Creek, Arizona, *Environ. Sci. Technol.*, *34*, 1150–1155.

Gundersen, J. K., and B. B. Jørgensen (1990), Microstructure of diffusive boundary layers and the oxygen uptake of the sea floor, *Nature*, *345*, 604–607.

Güss, S. (1998), Oxygen uptake at the sediment-water interface simultaneously measured using a flux chamber method and microelectrodes: Must a diffusive boundary layer exist?, *Estuarine Coastal Shelf Sci.*, *46*, 143–156.

Harvey, J. W., and K. E. Bencala (1993), The effect of streambed topography on surface-subsurface water exchange in mountain catchments, *Water Resour. Res.*, *29*, 89–98.

Harvey, J. W., and C. C. Fuller (1998), Effect of enhanced manganese oxidation in the hyporheic zone on basin-scale geochemical mass balance, *Water Resour. Res.*, *34*, 623–636.

Harvey, J. W., M. H. Conklin, and R. S. Koelsch (2003), Predicting changes in hydrologic retention in an evolving semi-arid alluvial stream, *Adv. Water Resour.*, *26*, 939–950.

Huettel, M., W. Ziebis, and S. Forster (1996), Flow-induced uptake of particulate matter in permeable sediments, *Limnol. Oceanogr.*, *41*, 309–322.

Huettel, M., H. Røy, E. Precht, and S. Ehrenhauss (2003), Hydrodynamical impact on biogeochemical processes in aquatic sediments, *Hydrobiologia*, *494*, 231–236.

Iversen, N., and B. B. Jørgensen (1993), Diffusion coefficients of sulfate and methane in marine sediments: Influence of porosity, *Geochim. Cosmochim. Acta*, *57*, 571–578.

Jones, J. B., S. G. Fisher, and N. B. Grimm (1995), Vertical hydrolgic exchange and ecosystem metabolism in a Sonoran Desert stream, *Ecology*, *76*, 942–952.

Lai, J. L., S. L. Lo, and C. F. Lin (1994), Effects of hydraulic and medium characteristics on solute transfer to surface runoff, *Water Sci. Technol.*, *30*, 145–155.

Manes, C., D. Pokrajac, I. McEwan, V. Nikora, and L. Campbell (2006), Application of UVP within porous beds, *J. Hydraul. Eng.*, *132*, 983–986.

Marinelli, R. L., R. A. Jahnke, D. B. Craven, J. R. Nelson, and J. E. Eckman (1998), Sediment nutrient dynamics on the South Atlantic Bight continental shelf, *Limnol. Oceanogr.*, *43*, 1305–1320.

Marion, A., and M. Zaramella (2005), Diffusive behavior of bedform-induced hyporheic exchange in rivers, *J. Environ. Eng.*, *131*, 1260–1266.

Marion, A., M. Bellinello, I. Guymer, and A. Packman (2002), Effect of bed form geometry on the penetration of nonreactive solutes into a streambed, *Water Resour. Res.*, *38*(10), 1209, doi:10.1029/2001WR000264.

Meysman, F. J. R., O. S. Galaktionov, P. L. M. Cook, F. Janssen, M. Huettel, and J. J. Middelburg (2007), Quantifying biologically and physically induced flow and tracer dynamics in permeable sediments, *Biogeosciences*, *4*, 627–646.

Mulholland, P. J., et al. (2001), Inter-biome comparison of factors controlling stream metabolism, *Freshwater Biol.*, *46*, 1503–1517.

Nagaoka, H., and S. Ohgaki (1990), Mass transfer mechanism in a porous riverbed, *Water Res.*, *24*, 417–425.

Nezu, I., and H. Nakagawa (1993), *Turbulence in Open-Channel Flows*, A. A. Balkema, Brookfield, Vt.

Nielsen, L. P., P. B. Christensen, N. P. Revsbech, and J. Sørensen (1990), Denitrification and photosynthesis in stream sediment studied with microsensor and whole-core techniques, *Limnol. Oceanogr.*, *35*(5), 1135–1144.

O'Connor, B. L., and M. Hondzo (2008a), Dissolved oxygen transfer to sediments by sweep and eject motions in aquatic environments, *Limnol. Oceanogr.*, *53*, 566–578.

O'Connor, B. L., and M. Hondzo (2008b), Enhancement and inhibition of denitrification by fluid-flow and dissolved oxygen flux to stream sediments, *Environ. Sci. Technol.*, *42*, 119–125.

O'Connor, B. L., M. Hondzo, D. Dobraca, T. M. LaPara, J. C. Finlay, and P. L. Brezonik (2006), Quantity-activity relationship of denitrifying bacteria and environmental scaling in streams of a forested watershed, *J. Geophys. Res.*, *111*, G04014, doi:10.1029/2006JG000254.

Packman, A. I., and J. S. MacKay (2003), Interplay of stream-subsurface exchange, clay particle deposition, and streambed evolution, *Water Resour. Res.*, *39*(4), 1097, doi:10.1029/2002WR001432.

Packman, A. I., and M. Salehin (2003), Relative roles of stream flow and sedimentary conditions in controlling hyporheic exchange, *Hydrobiologia*, *494*, 291–297.

Packman, A. I., N. H. Brooks, and J. J. Morgan (2000), Kaolinite exchange between a stream and streambed: Laboratory experiments and validation of a colloid transport model, *Water Resour. Res.*, *36*, 2363–2372.

Packman, A. I., M. Salehin, and M. Zaramella (2004), Hyporheic exchange with gravel beds: Basic hydrodynamic interactions and bedform-induced advective flows, *J. Hydraul. Eng.*, *130*, 647–656.

Peterson, B. J., et al. (2001), Control of nitrogen export from watersheds by headwater streams, *Science*, *292*, 86–90.

Rehg, K. J., A. I. Packman, and J. Ren (2005), Effects of suspended sediment characteristics and bed sediment transport on streambed clogging, *Hydrol. Processes*, *19*, 413–427, doi:10.1002/hyp.5540.

Reimers, C. E., R. A. Jahnke, and L. Thomsen (2001), In situ sampling in the benthic boundary layer, in *The Benthic Boundary Layer: Transport Processes and Biogeochemistry*, edited by B. P. Boudreau and B. B. Jørgensen, chap. 10, pp. 245–268, Oxford Univ. Press, London.

Reimers, C. E., H. A. Stecher III, G. L. Taghon, C. M. Fuller, M. Huettel, A. Rusch, N. Ryckelynck, and C. Wild (2004), In situ measurements of advective solute transport in permeable shelf sands, *Cont. Shelf Res.*, *24*, 183–201.

Ren, J., and A. I. Packman (2004), Stream-subsurface exchange of zinc in the presence of silica and kaolinite colloids, *Environ. Sci. Technol.*, *38*, 6571–6581, doi:10.1021/es035090x.

Revsbech, N. P., B. B. Jørgensen, and O. Brix (1981), Primary production of microalgae in sediments measured by oxygen microprofile, $H^{14}CO_3^-$ fixation, and oxygen exchange methods, *Limnol. Oceanogr.*, *26, 717–730.*

Revsbech, N. P., B. Madsen, and B. B. Jørgensen (1986), Oxygen production and consumption in sediments determined at high spatial resolution by computer simulation of oxygen microelectrode data, *Limnol. Oceanogr.*, *31*, 293–304.

Revsbech, N. P., J. P. Jacobsen, and L. P. Nielsen (2005), Nitrogen transformations in microenvironments of river beds and riparian zones, *Ecol. Eng.*, *24*, 447–455.

Richardson, C. P., and A. D. Parr (1988), Modified Fickian model for solute uptake by runoff, *J. Environ. Eng.*, *114*, 792–809.

Rothman, D. H., and D. C. Forney (2007), Physical model for the decay and preservation of marine organic carbon, *Science*, *316*, 1325–1328.

Røy, H., M. Hüttel, and B. B. Jørgensen (2002), The role of small-scale sediment topography for oxygen flux across the diffusive boundary layer, *Limnol. Oceanogr.*, *47*(3), 837–847.

Ruff, J. F., and L. W. Gelhar (1972), Turbulent shear flow in porous boundary, *J. Eng. Mech.*, *98*, 975–991.

Salehin, M., A. I. Packman, and M. Paradis (2004), Hyproheic exchange with heterogeneous streambeds: Laboratory experiments and modeling, *Water Resour. Res.*, *40*, W11504, doi:10.1029/2003WR002567.

Savant, S. A., D. D. Reible, and L. J. Thibodeaux (1987), Convective transport within stable river sediments, *Water Resour. Res.*, *23*, 1763–1768.

Thamdrup, B., H. Fossing, and B. B. Jørgensen (1994), Manganese, iron, and sulfur cycling in a coastal marine sediment, Aarhus Bay, Denmark, *Geochim. Cosmochim. Acta*, *58*, 5115–5129.

Thibodeaux, L. J., and J. D. Boyle (1987), Bedform-generated convective transport in bottom sediment, *Nature*, *325*, 341–343.

Tonina, D., and J. M. Buffington (2007), Hyporheic exchange in gravel bed rivers with pool-riffle morphology: Laboratory experiments and three-dimensional modeling, *Water Resour. Res.*, *43*, W01421, doi:10.1029/2005WR004328.

van Rijn, L. C. (1984), Sediment transport, part III: Bed forms and alluvial roughness, *J. Hydraul. Eng.*, *110*, 1733–1754.

Venkataraman, P., and P. Rama Mohan Rao (1998), Darcian, transitional, and turbulent flow through porous media, *J. Hydraul. Eng.*, *124*, 840–846.

Woessner, W. W. (2000), Stream and fluvial plain ground water interactions: Rescaling hydrogeologic thought, *Ground Water*, *38*, 423–429.

Zarnetske, J. P., M. N. Gooseff, T. R. Brosten, J. H. Bradford, J. P. McNamara, and W. B. Bowden (2007), Transient storage as a function of geomorphology, discharge, and permafrost active layer conditions in Arctic tundra streams, *Water Resour. Res.*, *43*, W07410, doi:10.1029/2005WR004816.

Zhou, D., and C. Mendoza (1993), Flow through porous bed of turbulent stream, *J. Eng. Mech.*, *119*, 365–383.

J. W. Harvey and B. L. O'Connor, U.S. Geological Survey, Mail Stop 430 National Center, Reston, VA 20192, USA. (jwharvey@usgs.gov; boconnor@usgs.gov)